CONF-750344--2

LA-UR -75-880

TITLE: PRELIMINARY DESIGN AND PERFORMANCE OF AN ADVANCED GAMMA RAY SPECTROMETER FOR FUTURE ORBITER MISSIONS

AUTHOR(S): A. E. Metzger, R. H. Parker, J. R. Arnold, R. C. Reedy, and J. I. Trombka

SUBMITTED TO: Proceedings of the 6th Lunar Science Conference, Houston, Texas, March 17-21, 1975.

MASTER

los alamos
scientific laboratory
of the University of California
LOS ALAMOS, NEW MEXICO 87544

Form No. 836
St. No. 2629
1/75

UNITED STATES
ENERGY RESEARCH AND
DEVELOPMENT ADMINISTRATION
CONTRACT W-7405-ENG. 36

PRELIMINARY DESIGN AND PERFORMANCE OF AN ADVANCED GAMMA RAY SPECTROMETER FOR FUTURE ORBITER MISSIONS

A. E. Metzger and R. H. Parker
Jet Propulsion Laboratory
Pasadena, California 91103

J. R. Arnold
University of California, San Diego
La Jolla, California 92037

R. C. Reedy
Los Alamos Scientific Laboratory
Los Alamos, New Mexico 87544

J. I. Trombka
Goddard Space Flight Center
Greenbelt, Maryland 20771

ABSTRACT

A knowledge of the composition of planets, satellites and asteroids is of primary importance in understanding the formation and evolution of the solar system. Gamma-ray spectroscopy is capable of measuring the composition of meter-depth surface material from orbit around any body possessing little or no atmosphere. Measurement sensitivity is determined by detector efficiency and resolution, counting time and the background flux, while the effective spatial resolution depends upon the field-of-view and counting time together with the regional contrast in composition. The advantages of using germanium as a detector of gamma rays in space are illustrated experimentally and a compact instrument cooled by passive thermal radiation is described. Calculations of the expected sensitivity of this instrument at the Moon and Mars show that at least a dozen elements will be detected, twice the number which have been isolated in the Apollo gamma-ray data.

OBJECTIVES

Given the necessary capabilities and suitable characteristics, well-planned orbital missions provide the opportunity of examining the entire surface of a planetary, satellite, or asteroidal body. The contrasting interpretations of the surface history of Mars derived from the Mariner 9 orbiter and the preceding flyby missions of limited coverage illustrate the importance of a comprehensive global survey. From among the measurables, a knowledge of composition is one of the most important parameters with which to characterize the nature and evolution of a planetary body.

A gamma-ray spectroscopy experiment for the purpose of measuring the composition of surface material can be undertaken from an orbit around any planet or satellite body possessing little or no atmosphere, and where the instrument is not situated within a trapped radiation belt characterized by intense fluxes in the MeV range. The effective sampling depth is on the order of half a meter. Atmospheric thicknesses greater than 50-100g/cm^2 will absorb too much of the surface gamma ray flux; it may be noted that the Martian atmosphere is an order of magnitude more tenuous than this.

A flux of gamma rays originates at the surface of any condensed object in the solar system from the decay of the primordial radioactive nuclei as well as the interaction of matter with cosmic rays and their secondary products. Since a portion of this gamma-ray flux will consist of discrete lines which are characteristic of the emitting nuclei, measurement of the energy spectrum over a range of 0.2-10 MeV with adequate energy resolution will yield concentrations of elements for which this characteristic emission is sufficiently intense and upper limits for elements where it is not. The principal agents for the production of induced gamma ray lines from cosmic rays are secondary neutrons. Fast and thermal neutrons

undergo inelastic scattering, capture and activation reactions, whose radioactive products decay with a range of half-lives. During solar flares, the great enhancement of energetic solar particle fluxes will result in activation reactions, some with half lives sufficiently long to be observed subsequent to the flare when the solar background has diminished. A solar component will be observable during missions lasting on the order of months, particularly at Mercury, where the solar particle fluxes are increased (as the inverse square of the distance) by proximity to the Sun. A fuller discussion of these mechanisms can be found in Reedy and Arnold, (1972), and Reedy, Arnold, and Trombka (1973).

The bulk composition of a planetary body can be determined directly from its surface composition only if the body has accumulated uniformly and remained undifferentiated, a pattern of development which now appears unlikely for any body of significant size. However, as terrestrial and lunar studies have demonstrated, a knowledge of surface rock materials permits conclusions to be drawn not only about bulk composition, but also with regard to the nature of the differentiation process the object has undergone and the resultant distribution of elements between crust, mantle and core. The Apollo orbiting gamma ray spectrometer and x-ray spectrometer experiments have demonstrated how regional variations of rock type can be mapped from orbit on the basis of element concentrations and correlated with surface morphology (Trombka et al. 1973, Adler et al 1972). By measuring the composition of various bodies in the solar system, it will be possible to learn how the relative abundances of many volatile and refractory elements vary with distance from the Sun. These comparisons will serve as indicators of the conditions which prevailed in the clouds of dust and gas of the solar nebula from which these bodies accreted.

Based on contemporary knowledge and the anticipated capability of gamma ray spectroscopy (which will be discussed in some detail below), we can summarize

some of the major objectives for possible future orbiting experiments. Carried on a lunar polar orbiter, a gamma ray spectrometer would map the whole of the lunar surface with greater sensitivity than the 20% of the surface covered by the Apollo experiment. The experiment would search for provinces containing possibly unrecognized major rock types, establish the moon-wide distribution of presently known rock types such as KREEP, relate composition to other local parameters such as morphology, albedo and elevation, and look for primitive volatile constituents which possibly exist at the poles. On a Mars polar orbiter, a gamma ray spectrometer would study the volcanic shield and plains materials, determine if the surface rocks were rich in the more volatile elements, look for compositional contrasts between the heavily cratered and relatively smooth areas, try to determine the nature of the eolian deposits, and investigate both the composition and seasonal variations of the polar caps. The surface of Mercury raises questions of comparative composition with the lunar highlands, the nature of the tectonic processes which appear in Mariner 10 photographs, and the partitioning of elements with depth in this planet of high specific gravity. Looking toward more distant missions, recent evidence indicates that significant compositional variation exists among the satellites of the outer planets, the knowledge of which will bear on the environment for condensation and the evolutionary sequence in the outer portions of the solar nebula (Fanale, Johnson and Matson, 1974). Asteroid and comet missions have also been contemplated, where gamma-ray spectroscopy may be used to explore an evident diversity of compositions, a prime objective being to determine which objects may be parent bodies or otherwise related to various meteorite classes (Chapman and Salisbury, 1973). These smaller bodies are probably not extensively differentiated. If this is true, the surface composition will represent the bulk. This

investigation might also contribute to recognizing the source or sources of objects which heavily bombarded the Moon, and apparently Mercury and Mars as well, during the first 0.6 Gy of the Solar System.

SPATIAL RESOLUTION

The spatial resolution of a gamma-ray spectrometer in orbit will be determined by a combination of two factors, the field-of-view and counting statistics.

Field-of-View

Figure 1 illustrates the angular dependence of the response of an omnidirectional detector at an altitude of 100km above the surface of the Moon. For a given detector-source distance ℓ, photons striking the detector are emitted at a fixed angle β from the normal at the source, and strike the detector at an angle θ with respect to the line connecting the detector and the center of the moon. The limiting distance, ℓ_{max}, is the horizon distance, equal to $(2Rh+h^2)^{\frac{1}{2}}$. For a height of 100km above the moon surface, ℓ_{max} is 598km.

By integrating the intensity per unit source area at the detector over the radius of the region viewed and the moon's surface area at each radius, one can calculate the flux at the detector originating within a circle of radius ρ centered at the subsatellite point on the Moon's surface. The calculations shown in Figure 1 were done for four sources of gamma rays: an (n,γ) reaction (the 4.936 MeV line from $Si(n,\gamma)$), an $(n,x\gamma)$ reaction, (the 1.369 MeV from $Mg(n,n\gamma)$), a source uniform with depth (any natural radioactive decay line), and a solar cosmic ray (SCR)-produced radionuclide (the 1.809 MeV line of Al^{26} produced by protons on Si). The difference among these cases is the distribution in the first few photon mean free paths of the surface; gamma ray production increases considerably with depth near the surface for the (n,γ)

reaction, increases somewhat with depth for the (n, xγ) reaction, and decreases rapidly with depth for the SCR case. The relative fractions of the flux at an isotropic detector 100km above the lunar surface, are given in the figure for a point source, inside a circle of uniform distribution, and beyond a boundary for each of these four cases.

For the source uniformly distributed with depth and a detector altitude of 100km, the distance ρ where I' falls to half the value of the point source at the subdetector point is 73km. From a source uniformly distributed in area, half the flux at the detector originates inside a circle of radius 118km. At 68km from a great circle boundary, 75% of the field-of-view is occupied by the region below the detector and 25% by the region beyond the boundary. Corresponding distances for the SCR case are considerably greater than these. For the (n,xγ) and (n,γ) cases these distances are about 90% and 80%, respectively, of those of the uniform case. The galactic cosmic ray-produced radionuclides vary between the uniform case and the (n,xγ) case depending on the excitation function for the reaction.

The Apollo gamma ray results for the western maria areas, where there is a well defined distinction in thorium concentration with the surrounding highlands, have confirmed the calculations shown in Figure 1. Where the contrast in concentration is significant, a spatial resolution on the order of 60km (2°) at an altitude of 110km has been obtained.

The field-of-view can be narrowed by providing an active anticoincidence collimator around and in front of the central detector but the weight requirement is substantial because of the increasing penetration of gamma rays up to several MeV. In addition, by limiting the field-of-view, the counting time required to acquire satisfactory statistics over a particular area is proportionally increased. The appeal of a collimator increases with increasing altitude in orbit,

and with the increasing availability of data gathering time.

Counting Time

The concentration of an element is derived from the pulse height spectrum generated by the interaction of its emitted lines with the detector, using either the full functional response or its photopeak. In either case, since the counting process is statistical, an adequate number of events must be detected in order to determine the fraction due to a particular reaction in the presence of many others and above a strong, featureless continuum. The latter is generated principally by cosmic ray cascade processes in the lunar or planetary surface but processes of Compton scattering and bremsstrahlung also contribute. Local interactions and the cosmic gamma ray flux are additional background components. It is necessary, therefore, to accumulate data for a minimum of 0.5-1 hour over each unit of spatial resolution to obtain sufficient statistics for a reasonably complete analysis. Meaningful determinations can be made of several elements with less counting time, while others require longer periods to achieve sensitivities of geological significance. All benefit from longer periods of sampling.

The relationship between the effective field-of-view and counting statistics which determines the actual spatial resolution can be illustrated by the following example. If six months of data, gathered uniformly over the lunar surface at a mean altitude of 110km with an orbit period of 2 hr is assumed, the spacecraft will make 2190 orbits while acquiring data, and the average time per 60kmx60km area units of effective resolvability (ignoring the effect of latitude) will be about 1500 sec. But for a spacecraft in polar orbit, the higher the latitude of observation, the greater the measurement time obtained. Specifically, the time over a 60km x 60km polar unit will be 24 hours, compared

to 470 sec for an equatorial unit of the same size. It will therefore be necessary to group several equatorial units to obtain sufficient statistics for a nominal analysis. The experiment would then be time-limited in spatial resolution to roughly 5^{o} at the equator and $3\frac{1}{2}^{o}$ at 60^{o} latitude, but field-of-view-limited towards the pole. It is noteworthy that at lower latitudes, six months of uniformly distributed operations will not exhaust the point of useful data return. As the orbital altitude is decreased, the field-of-view is diminished and therefore the spatial resolution will improve, but only over those regions for which sufficient counting time is available.

INSTRUMENT DESIGN

The Apollo gamma-ray spectr eter (AGRS) consisted of a 7cmx7cm cylindrical NaI(Tl) detector surrounded by a plastic scintillator to reject charged particle events. Five hundred and twelve channels of pulse height conversion were used to span a nominal energy range of 0.2-10 MeV (Harrington et al, 1974). The energy resolutions of the NaI(Tl) detectors were in the range of 7.5-8.5% for the 0.66 MeV gamma ray line of Cs-137. This is close to the best resolution which can be achieved with scintillators and,in a sense, is a culmination of their application to lunar gamma ray spectroscopy, which began with a CsI(Tl) detector in the Ranger gamma ray spectrometer having a resolution of 12.5-13%, followed by the Russian experiment on Luna 10 which first detected gamma rays from the Moon in the mid-60s using a NaI(Tl) detector with a resolution of about 10% (Vinogradov et al, 1967).

The direction of substantial improvement beyond the performance of the Apollo inst at lies in the use of germanium (Ge) detectors. Germanium detectors are capable of an energy resolution some 40 times greater than the NaI scintillators used to date. The advantages of superior resolution which lead to a more sensitive compositional analysis take two forms, 1) the ability to better discriminate a gamma ray peak from the background flux and, 2) the ability to distinguish gamma ray lines which are closely adjacent in energy. These characteristics are illustrated by an experimental comparison between the response of the Apollo NaI detector and a 28cc Ge(Li) detector shown in Figures 2 and 3. Figure 2 illustrates the comparative response to the principal thorium line at 2.61 MeV. The NaI detector experiment was set up to duplicate the peak-to-background ratio observed by the Apollo gamma ray spectrometer for the average lunar spectrum at 2.61 MeV, where the featureless continuum under the characteristic

gamma ray line makes up about 85% of the total flux detected. The Ge(Li) test was subsequently run with the same geometry. It is seen that in the Ge detector spectrum, the photopeak is much more readily distinguishable from the background. Figure 3 compares a portion of the same spectrum around 1.4 MeV. The Ge detector demonstrates the capability of resolving gamma ray lines due to Co-60 (1.332 MeV) and an unidentified line at 1.43 MeV associated with the Cf-252 source, neither of which can be distinguished from the dominant 1.46 MeV K-40 background line in the response of the NaI detector.

The advanced gamma ray spectrometer will utilize a single intrinsic (high purity) Ge detector with a minimum volume of 50cc, corresponding to an efficiency of at least 15% of a 7.6cm (3") NaI detector to a 1.33 MeV gamma ray, and hopefully as large as 100cc, a size which has already been fabricated. The detector will be hermetically sealed to avoid contamination. The use of an intrinsic detector removes the requirements for continuous cooling and allows a passive thermal radiator system, modeled after designs which have been successfully employed for infrared detectors on satellites, to be used to provide the necessary cooling during operation. Use of a passive radiator rather than a mechanical cooler or a refrigerator system, will allow the weight and volume of this spectrometer to be comparable to that of the Apollo instrument. To take advantage of the improved resolution offered by the Ge detector, at least 4096 and preferably 8192 channels of pulse height analysis are required.

The avoidance of inherent sources of detectable radiation on the spacecraft is essential. An RTG represents an extreme example. Insofar as it is practical, the proximate use of materials which will undergo induced reactions leading to the same characteristic lines as those being measured from the planetary body should be minimized.

The design of this system is proceeding. It is intended that this instrument be applicable to an experiment at Mars as well as the Moon. Since a Mars orbiter would be constrained to altitudes on the order of 1000 km due to planetary quarantine, a collimator which would reduce the spatial resolution by a factor of 4 in area might be a desirable addition. The intention is to provide for this possibility as an option. There is also reason to believe that this same system may also be used in orbiting Mercury by placing a sun shade over the instrument, a concept which proved itself in the Mariner 10 mission. A closer look at this latter possibility is planned.

EXPERIMENTAL

A program of experimental studies to supplement calculations of expected performance and to examine the properties of intrinsic Ge detectors has begun. The experiments make use of a Cf-252 neutron source to initiate the inelastic neutron scattering and neutron capture reactions leading to characteristic gamma ray emission. The Cf-252 source also produces a background used in simulating the featureless continuum arising from cosmic ray cascade processes which will underlie any gamma ray line spectrum observed in orbit. The data of Figures 2 and 3 were obtained with characteristic lines derived from a Th-228 source plus residual laboratory background. The proper Th/continuum ratio , which duplicated the Apollo lunar data, was established by a suitable separation between the Cf-252 source and the NaI detector.

A preliminary example of the induced line spectra produced by the Cf-252 neutron flux incident on an Fe target is given in Figures 4 and 5. In this experiment the Fe target was placed in close proximity to the source, both being within a container filled with water and lined with borax. This has the effect

of emphasizing the thermal component of the neutron flux; some measurements have also been made without the water moderator but the fast neutron flux is still depleted relative to cosmic ray secondary production and a set of experiments are planned with a fast neutron source. The detector used in these experiments is a high performance intrinsic device with a volume of 50cc, an efficiency relative to a 7.6cm (3") NaI detector at 1.33 MeV greater than 15% and 2.0 keV resolution. It was grown and fabricated at the Lawrence Berkeley Laboratory (see, for example, Pehl, Cordi and Goulding, 1972).

The spectrum of Figure 4 contains all the significant neutron capture lines expected. The multiplicity of characteristic lines which can be observed enhances the ease of identifying a given element. This is particularly true for the first and second escape peaks which lie precisely 0.511 MeV and 1.022 MeV respectively below the photopeak energy. By using the combined statistics of all the major lines, the sensitivity of detection is increased. Compared to the Moon, the continuum underlying Figure 4 is a factor of 2-3 greater at low energies and lower at high energies. This difference is easily taken into account when using the laboratory results to predict those expected for the flight experiment; a greater challenge is the need to either reproduce in the laboratory the spectrum of secondary neutrons calculated for and observed at the lunar surface (Lingenfelter, Canfield and Hampel, 1972; Burnett & Woolum, 1974) or to normalize the laboratory spectrum accordingly.

CALCULATED RESPONSES

It is possible to make a more quantitative comparison of the relative responses of the NaI and Ge(Li) detectors to the 2.61 MeV Th line shown in Figure 2. While this feature is recognized much more readily in the Ge(Li) spectrum, the relative efficiencies of the detectors, which will be reflected in the total number of counts detected, must also be considered. If C_t is the total number of counts in the peak interval, B_t the background count in the peak interval, and N the net (peak) count in the peak interval, then

$$N = C_t - B_t \tag{1}$$

and

$$MDL_{n\sigma} = \frac{n\sqrt{C}}{N} \tag{2}$$

where MDL is the minimum detectable limit and n is the statistical significance which will be set at 3σ. Since the counting times were the same in this experiment, a reduction to rates is not necessary. Inspection of the flat, broad peak response for the NaI detector indicates that it extends over 7 channels with N(NaI) = 2150 counts and B_t(Na) = 30,600 counts so that from Eq. (2) the $MDL_{3\sigma} = 3 \times \frac{\sqrt{30600}}{2150} = 0.24$ parts of whatever concentration was being detected in this measurement. By comparison, the Ge response shows a net peak and background total over the two principal channels of 99 and 249 counts respectively so that for the Ge detector the $MDL_{3\sigma} = 3 \times \frac{\sqrt{249}}{99} = 0.48$ parts of the same concentration that was measured with the AGRS detector. The ratio of detectabilities shows that the NaI detector is a factor of 2 more sensitive in this case, but it must be remembered that the Ge(Li) detector is only 28cc in volume and 50cc is considered the minimum acceptable size. Furthermore, this assumes an accurate determination of both backgrounds, but as can be seen from the

figure, separation of the continuum from the total response is much more difficult for the NaI detector than the Ge. This separation has, in fact, been the most formidable aspect of reducing the Apollo lunar gamma ray data (Metzger, et al., 1974).

Turning to the detection of gamma rays from the Moon, the (3σ) minimum detectable flux F_{min} can be calculated approximately from

$$F_{min} = \frac{n}{G\varepsilon\ (E)\Omega} \left(\frac{B\Delta E}{At}\right)^{\frac{1}{2}} \qquad (3)$$

where $\varepsilon(E)$ equals the photopeak efficiency at energy E, A is the effective area of the detector, t is the time of measurement, B is the background flux, ΔE is the full width half maximum (FWHM) of the photopeak, Ω is the lunar geometry factor, dependent on altitude, and G is the Gaussian factor which represents the fraction of the photopeak flux which falls within the FWHM of the detector's response. From F_{min} and S, the source function of characteristic gamma rays for a given reaction emitted through the lunar surface and measured in γ/cm^2-s per unit concentration of element Z, it is possible to compute $[Z]^t_{3\sigma\ MDL}$, the 3σ MDL of element Z for a given data accumulation time, from

$$[Z]^t_{3\sigma\ MDL} = \frac{F_{min}}{S} \qquad (4)$$

Values of S have been tabulated as fluxes from a semi-infinite plane based on a model of the cosmic ray interactions and gamma ray production mechanisms (Reedy, Arnold and Trombka, 1973). For the Th line at 2.61 MeV, S is 1.92×10^{-2} γ/cm^2-s-ppm while the background flux B at this energy is taken from a 7 hour Apollo average. With A = 44.9 cm^2, $\varepsilon(2.61)$ = .094, G = .76, Ω = .87 at an

altitude of 110 km and ΔE = .105MeV over the FWHM of the peak, we compute for 1 hour of counting (t=1 h):

$$B = 2.17 \times 10^{-2} \text{ c/cm}^2\text{s}, \quad F_{min} = 1.61 \times 10^{-2} \text{ } \gamma/\text{cm}^2\text{s}$$

and

$$(\text{Th})^{1\text{ h}}_{3\sigma\text{MDL}} = 0.90 \text{ ppm}$$

which is consistent with what has been observed in the analysis of Apollo data.

Applying the same considerations to the case of a Ge detector of approximate size 80cc, for which we take $\varepsilon(2.61) = 0.02$, $A = 27$ cm^2 and $E = 3.6$ keV, with the Apollo-derived background scaled to reflect both the narrower peak width and lower detector efficiency, the calculations yield $(\text{Th})^{1\text{ h}}_{3\sigma\text{MDL}} = 0.60$ ppm, 50% more sensitive than the AGRS detector.

The type of calculation just described has been extended to a set of elements to determine detectability with a single, large (approximately 80cc) intrinsic Ge detector. The energy resolution was taken to vary as $(E)^{-\frac{1}{2}}$ with energy, a relationship which is substantiated by laboratory measurements from 0.4 - 9 MeV. Correction factors were applied to take cognizance of the increase in detectability resulting from the presence of additional lines of significant strength relative to the prime line of each element, and from the contribution of the first escape peak over the energy range where the pair production process has a significant cross section (see Figure 5). The guidelines for developing this correction factor were:

1) Consideration was limited to two characteristic lines per element, the additional line being the second strongest which could be used.
2) A second line of equal intensity will increase the sensitivity of detection by $\sqrt{2}$ and lines of less intensity in proportion.

3) The first escape peak will increase sensitivity by a factor of 1 (no improvement) below 4MeV, $\sqrt{2}$ from 4-6 MeV, and 2 above 6 MeV.

For example, the 0.911 MeV gamma ray was chosen as the secondary line for thorium. Considering its yield relative to the 2.61 MeV line, detection efficiency, and the underlying continuum gave an enhancement factor (EF) of 1.15 bringing $(Th)^{1\ h}_{3\sigma MDL}$ to 0.60/1.15 = 0.52 ppm. In contrast, the two strongest lines of Fe are almost equal in intensity (Figure 5) so the line EF is $\sqrt{2}$. Each of these lines is above 6 MeV providing an escape peak EF of $2\sqrt{2}$, so the combined EF of both lines is $\sqrt{2}(2\sqrt{2}) = 4$. Interferences between lines, including both first and second escape peaks have also been considered and no lines within about two resolution widths of energy and possessing a relative intensity within an order of magnitude have been used.

The background flux for each characteristic energy has been derived from Apollo data, normalized to the FWHM energy width and efficiency of the Ge detector. The ability to remove the spacecraft-produced line component as an interference to the spectrum from the planetary body will be greater if measurements can also be made at large distances from the planetary body (e.g. in cislunar space) than if this correction must be computed theoretically. The following calculations assume this ability.

The results for the Moon are given in Table 1, together with an average soil analysis at three Apollo landing sites which are dominated by different rock components. The 3σ MDLs are calculated for altitude of 110 km, but the geometric factors for the moon and proportion of cosmic gamma ray flux contributed to the background vary over only a few percent at these low elevations. The analysis of Apollo data has yielded, for regional accumulations, on the order of one to several hours, results for Th, K, Fe, Ti, Si, O, and Mg (Metzger, et al., 1974); beside the same complement of elements with increased

sensitivity, use of the Ce detector will add U, Al, Ca, Na, Mn, and Lu. The ability to determine U independently of Th will make it possible to track possible variations in the Th/U ratio in regions of moderate to high radioactivity (Silver, 1974). Both Al and Ca are important in distinguishing among highland rock assemblages while the increased sensitivity for Ti will be particularly helpful in studying the degree of mixing at highland-mare interfaces. Other elements such as H, Ni, Cr, and Cl could be detected if regions of high concentration exist. There is a possibility of H in permafrost in permanently shadowed regions near the lunar pole.

Thorium and uranium together provide a special case in that the numerous lines of these elements dominate the characteristic spectrum below 2.75 MeV. Calculations show that the sensitivity of the integrated flux over a energy range from 0.55-2.75 MeV is 5.6 times greater than the 2.61 MeV photopeak alone. This has been utilized to calculate the distribution of radioactivity on a two degree regional scale from Apollo data (Trombka, et al., 1973).

A similar set of calculations is shown in Table 2 for the case of a Mars orbiter. The 3σ MDLs are above those of the lunar case because of the higher assumed altitude (1000 km), to which both the Mars and cosmic gamma ray background have been adjusted, and include the effect of atmospheric absorption, based on a mean surface density of 7 mb. Collimated and uncollimated values are given; in the former case fewer gamma rays are seen per unit time because of the reduced field-of-view. With collimation, more grouping of area units off the equator would be required to reach suitable levels of sensitivity for certain elements in exchange for the advantage of improved spatial resolution. The fact that many geologic regions are much larger than the resolvable area units makes it meaningful to consider observing periods on the order of 100

hours as applicable well away from the poles. This consideration applies to a long-live orbiting experiment on the Moon or Mercury as well as at Mars. In the case of Mars, the detectability of H and C is of prime importance because of the desire to determine both the composition and thickness of the polar caps and the possible presence of permafrost in adjacent regions.

The values of Tables 1 and 2 are appropriately conservative in that the MDLs are presented at the 3σ level, and by incorporating only two lines per element and ignoring the second escape peak of energetic gamma rays, only limited use has been made of the multiline associations available in the spectra of many of the elements. These calculations will eventually be repeated with updated values of detector efficiency, detector response characteristics, source functions, enhancement factors, etc., but the results presented here are believed accurate to a good first approximation.

SUMMARY

A gamma ray spectrometer of greater sensitivity and more straightforward in data analysis than the Apollo instrument is being designed around the use of an intrinsic Ge detector. This instrument will be capable of detecting more than a dozen elements, most of which are of prime geochemical significance. It is expected that the same basic instrument can be used at the Moon, Mars and Mercury. Calculations of sensitivity in terms of a 3σ MDL presented here are consistent with results from the Apollo gamma ray spectrometer, which used a NaI scintillation crystal, and with initial data from a program of experimental studies with a Ge detector. A satisfactory mission can be accomplished in 3-4 months, although operating periods on the order of a year are needed to fully utilize the capability in an orbit which covers essentially 100% of the lunar surface.

Acknowledgements

We wish to thank F. S. Goulding and R. H. Pehl at the Lawrence Berkeley Laboratory for making a large intrinsic Ge detector available to us. R. W. Campbell provided a neutron detection system for the laboratory experiments and M. Fong assisted in acquiring the data.

The work described in this paper was carried out in part under NASA contract, NAS 7-100 at the Jet Propulsion Laboratory, California Institute of Technology, and in part under an NASA contract, NAS 9-10670 at the University of California, San Diego

REFERENCES

Adler I., Trombka J., Gerard J., Lowman P., Schmadebeck R., Blodgett H., Eller E., Yin L., Lamothe R., Gorenstein P., and Bjorkholm P. (1972) "Apollo 15 Geochemical X-ray Fluorescence Experiment: Preliminary Report," Science 175, p. 436.

Burnett D. S., and Woolum D. S. (1974) "Lunar Neutron Capture as a Tracer for Regolith Dynamics," Proc. Fifth Lunar Science Conf. Supplement 5, Geochim. Cosmochim. Acta, Vol. 2, p. 2061, Pergamon.

Chapman, C. R., and Salisbury J. W. (1973) "Comparisons of Meteorite and Asteroid Spectral Reflectivities," Icarus 19, p. 507.

Panale F. P., Johnson T. V., and Matson D. L. (1974) "Io's Surface and the Histories of the Galilean Satellite," Planetary Satellites, Proceedings of the IAU Colloquium No. 28 (in press).

Harrington T. M., Marshall J. H.,Arnold J. R., Peterson L. P., Trombka J. I., and Metzger A. E. (1974) "The Apollo Gamma Ray Spectrometer," Nucl. Instr. & Methods, 118, p. 401.

Lingenfelter R. E., Canfield E. H., and Hampel V. E. (1972) "The Lunar Flux Revisited," Earth Planet. Sci. Lett. 16, p. 355.

Metzger A. E., Trombka J. I., Reedy R. C., and Arnold J. R. (1974) "Element Concentrations from Lunar Orbital Gamma-Ray Measurements," Proc. Fifth Lunar Science Conf., Supplement 5, Geochim. Cosmochim. Acta, Vol. 2, p. 1067, Pergamon.

Pehl R. H., Cordi R. H., and Goulding F. S. (1972) "High Purity Germanium: Detector Fabrication and Performance," IEEE Trans. Nucl. Sci., NS-19, No. 1, p. 265.

Reedy R. C. and Arnold J. R. (1972) "Interaction of Solar and Galactic Cosmic Ray Particles with the Moon," J. Geophys. Res., 77, p. 537.

Reedy R. C., Arnold J. R., and Trombka J. I. (1973) "Expected Gamma-Ray Emission Spectra from the Lunar Surface as a Function of Chemical Composition," J. Geophys. Res., 78, p. 5847.

Silver L. T. (1974) "Patterns of U-Th-Pb Distributions and Isotope Relations in Apollo 17 Soils," Abstracts of Papers submitted to the Fifth Lunar Science Conference, Part II, p. 706, The Lunar Science Institute.

Trombka J. I., Arnold J. R., Reedy R. C., Peterson L. E., and Metzger A. E. (1973) "Some Correlations Between Measurements by the Apollo Gamma-Ray Spectrometer and Other Lunar Observations," Proc. Fourth Lunar Sci. Conf., Geochim. Cosmochim. Acta, Suppl. 4, Vol. 3, p. 2847, Pergamon.

Vinogradov A. P., Surkov Yu. A., Chernov G. M., Kirnozov F. F., Nazarkina G. B. (1967) "Lunar Gamma-Radiation and the Composition of the Lunar Rocks According to the Results of a Luna-10 Experiment," Cosmic Res. USSR, Vol. 5, p. 741.

FIGURE CAPTIONS

Figure 1

The top diagram shows the angles (β and θ) and distances for a detector at an altitude h above the Moon relative to a point source on its surface. The graph shows the relative fluxes at an isotropic detector from a point source (I'), from inside a circle, and from beyond a great circle boundary as a function of the distance along the surface of the Moon from the subdetector point. The fluxes are for an altitude of 100 km above the Moon (R_M = 1738 km) and for four different profiles for γ ray source intensity versus depth.

Figure 2

Performance comparison in the detection of thorium gamma rays using the Apollo gamma ray spectrometer and a 28 cm^3 Ge(Li) detector in identical laboratory experiments.

Figure 3

Performance comparison in the detection of potassium as in Figure 2.

Figure 4

Gamma ray spectrum using Cf-252 neutrons in water to irradiate an Fe target. The error bars indicate the envelope of fluctuations around the hand fitted mean.

Figure 5

Detailed regions of Figure 4 showing the resolved lines at 7.6 MeV and the two sets of escape peaks. Also shown is an example of a low intensity line at 7.281 MeV which can be identified using the escape peaks.

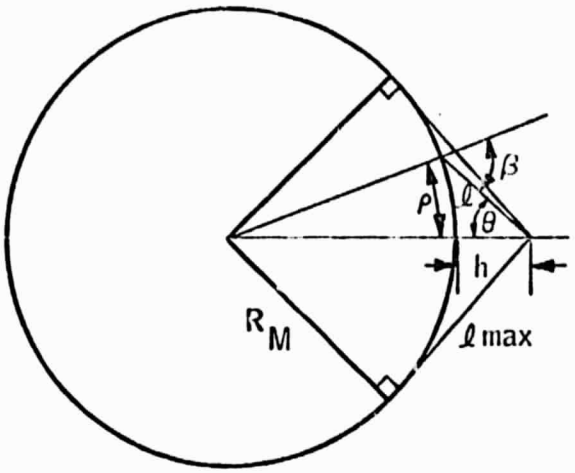
β
ρ
ℓ
θ
h
R M
ℓ max

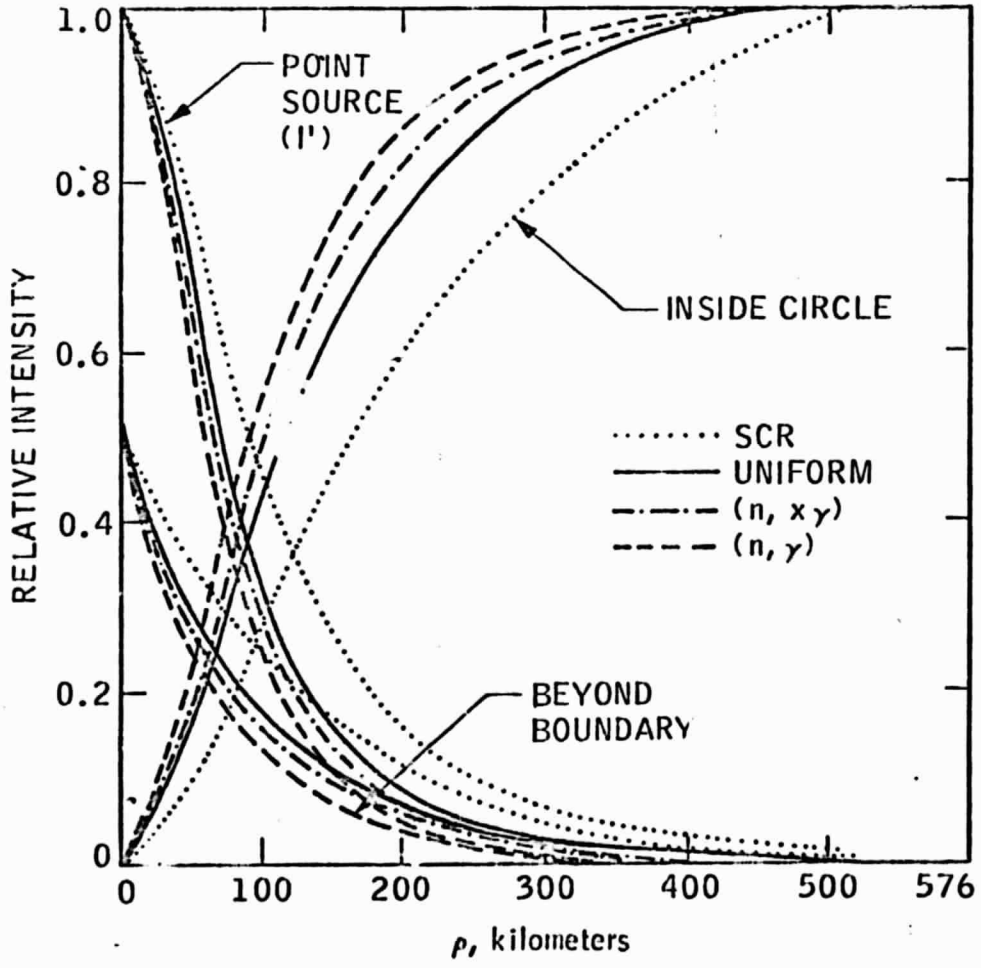
1.0
0.8
0.6
0.4
0.2
0
RELATIVE INTENSITY
POINT SOURCE (I')
INSIDE CIRCLE
SCR
UNIFORM
(n, xγ)
(n, γ)
BEYOND BOUNDARY
0
100
200
300
400
500
576
ρ, kilometers

Figure 1

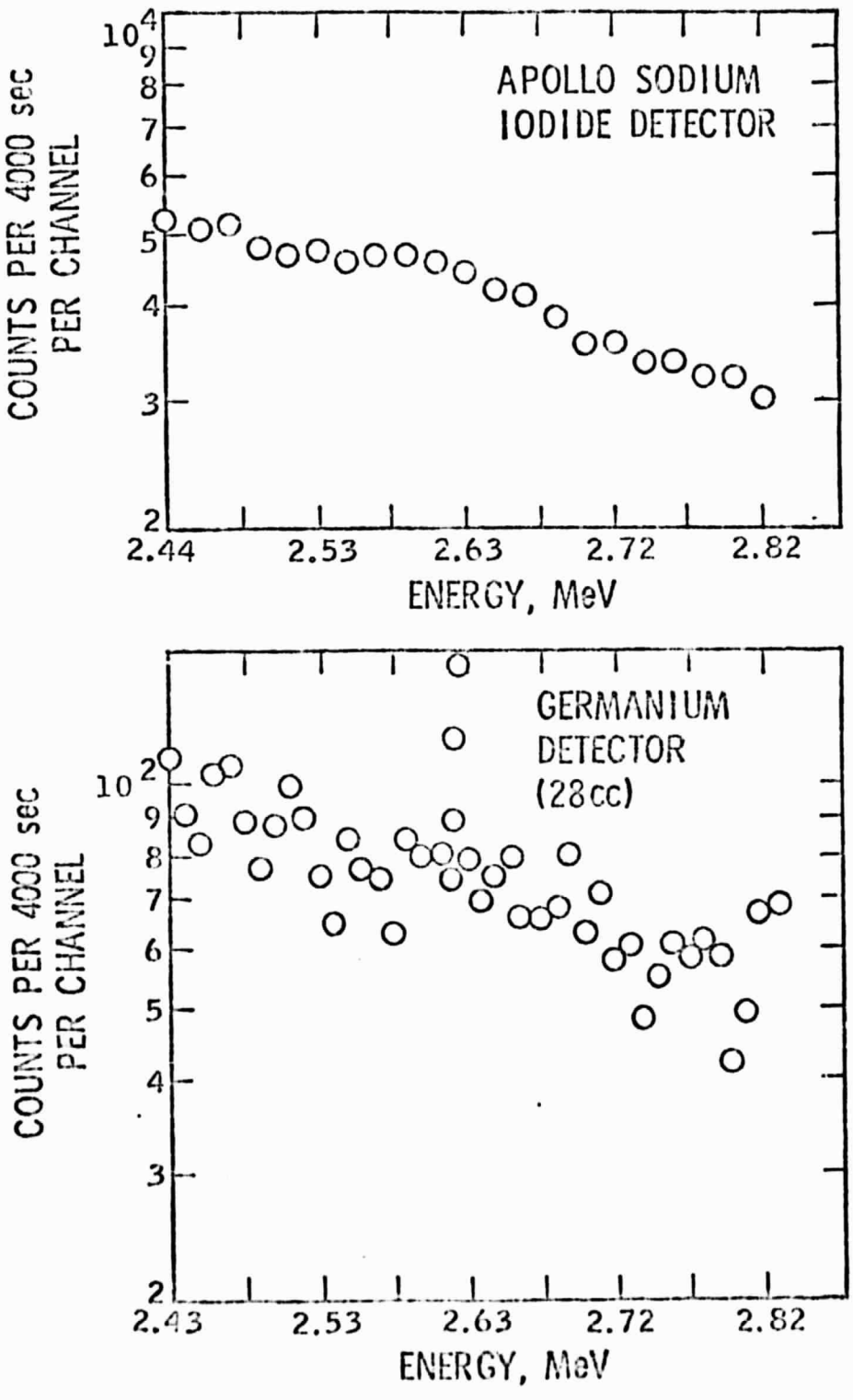
APOLLO SODIUM
IODIDE DETECTOR
COUNTS PER 4000 sec
PER CHANNEL
10^4
9
8
7
6
5
4
3
2
2.44
2.53
2.63
2.72
2.82
ENERGY, MeV
GERMANIUM
DETECTOR
(28cc)
COUNTS PER 4000 sec
PER CHANNEL
10^2
9
8
7
6
5
4
3
2
2.43
2.53
2.63
2.72
2.82
ENERGY, MeV

Figure 2

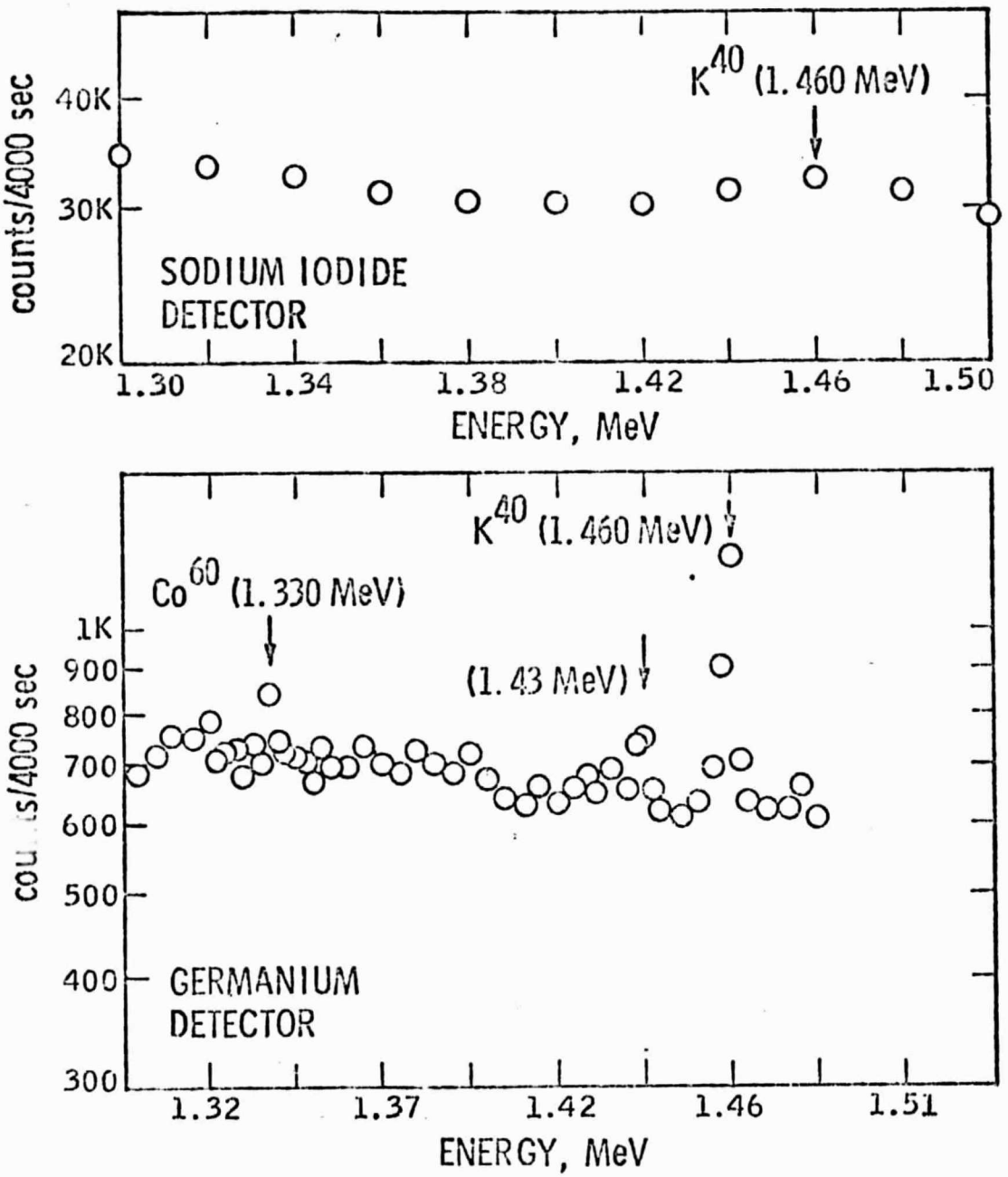
counts/4000 sec
40K
30K
20K
K^{40} (1.460 MeV)
SODIUM IODIDE
DETECTOR
1.30
1.34
1.38
1.42
1.46
1.50
ENERGY, MeV
K^{40} (1.460 MeV)
Co^{60} (1.330 MeV)
(1.43 MeV)
1K
900
800
700
600
500
400
300
GERMANIUM
DETECTOR
1.32
1.37
1.42
1.46
1.51
ENERGY, MeV

Figure 3

Figure 4

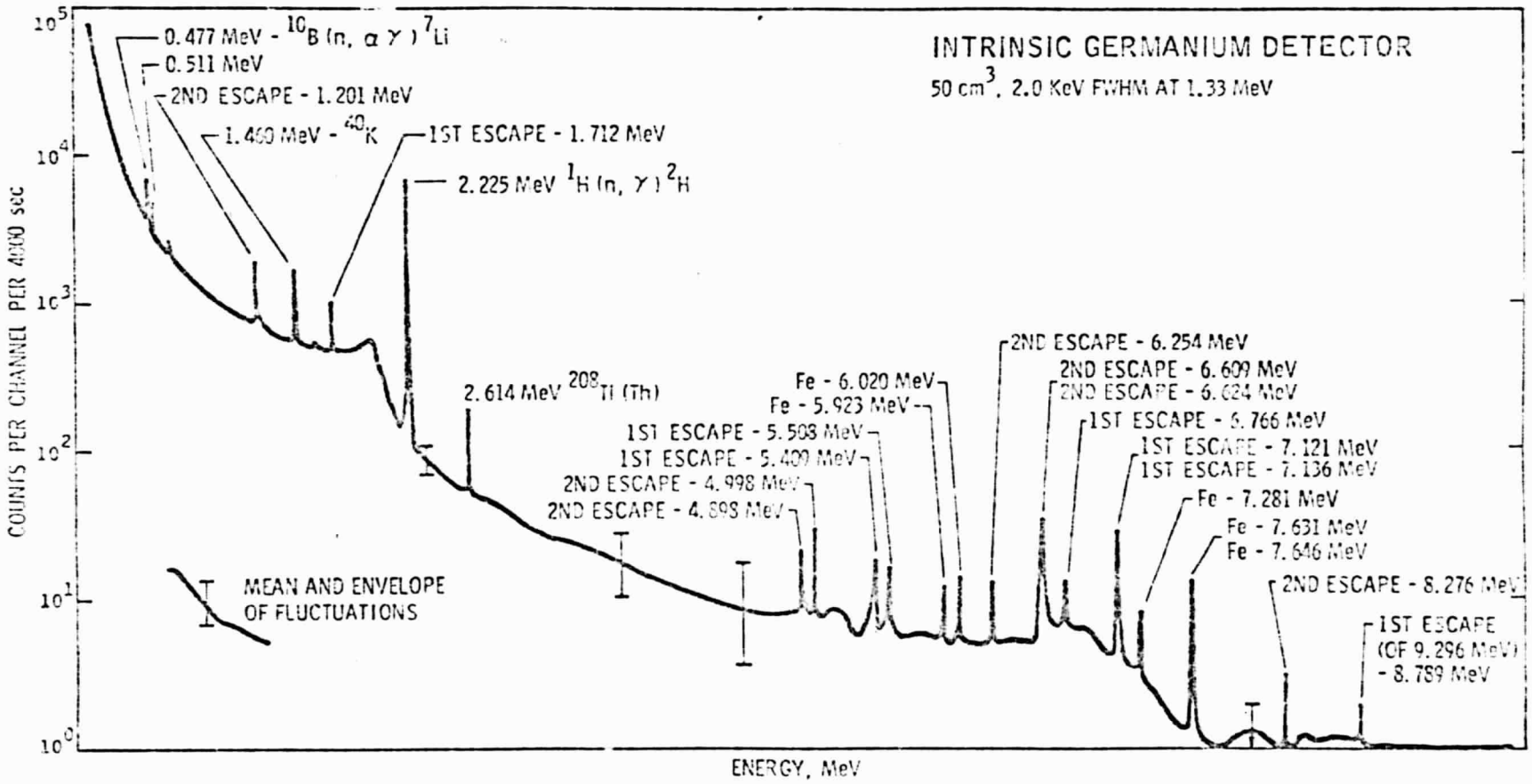
INTRINSIC GERMANIUM DETECTOR
50 cm^3, 2.0 KeV FWHM AT 1.33 MeV
COUNTS PER CHANNEL PER 4000 sec
ENERGY, MeV
10^5
10^4
10^3
10^2
10^1
10^0
0.477 MeV - ^{10}B (n, α γ) ^{7}Li
0.511 MeV
2ND ESCAPE - 1.201 MeV
1.460 MeV - ^{40}K
1ST ESCAPE - 1.712 MeV
2.225 MeV ^{1}H (n, γ) ^{2}H
2.614 MeV ^{208}Tl (Th)
Fe - 6.020 MeV
Fe - 5.923 MeV
1ST ESCAPE - 5.508 MeV
1ST ESCAPE - 5.409 MeV
2ND ESCAPE - 4.998 MeV
2ND ESCAPE - 4.898 MeV
2ND ESCAPE - 6.254 MeV
2ND ESCAPE - 6.609 MeV
2ND ESCAPE - 6.624 MeV
1ST ESCAPE - 6.766 MeV
1ST ESCAPE - 7.121 MeV
1ST ESCAPE - 7.136 MeV
Fe - 7.281 MeV
Fe - 7.631 MeV
Fe - 7.646 MeV
2ND ESCAPE - 8.276 MeV
1ST ESCAPE
(OF 9.296 MeV)
- 8.789 MeV
MEAN AND ENVELOPE
OF FLUCTUATIONS

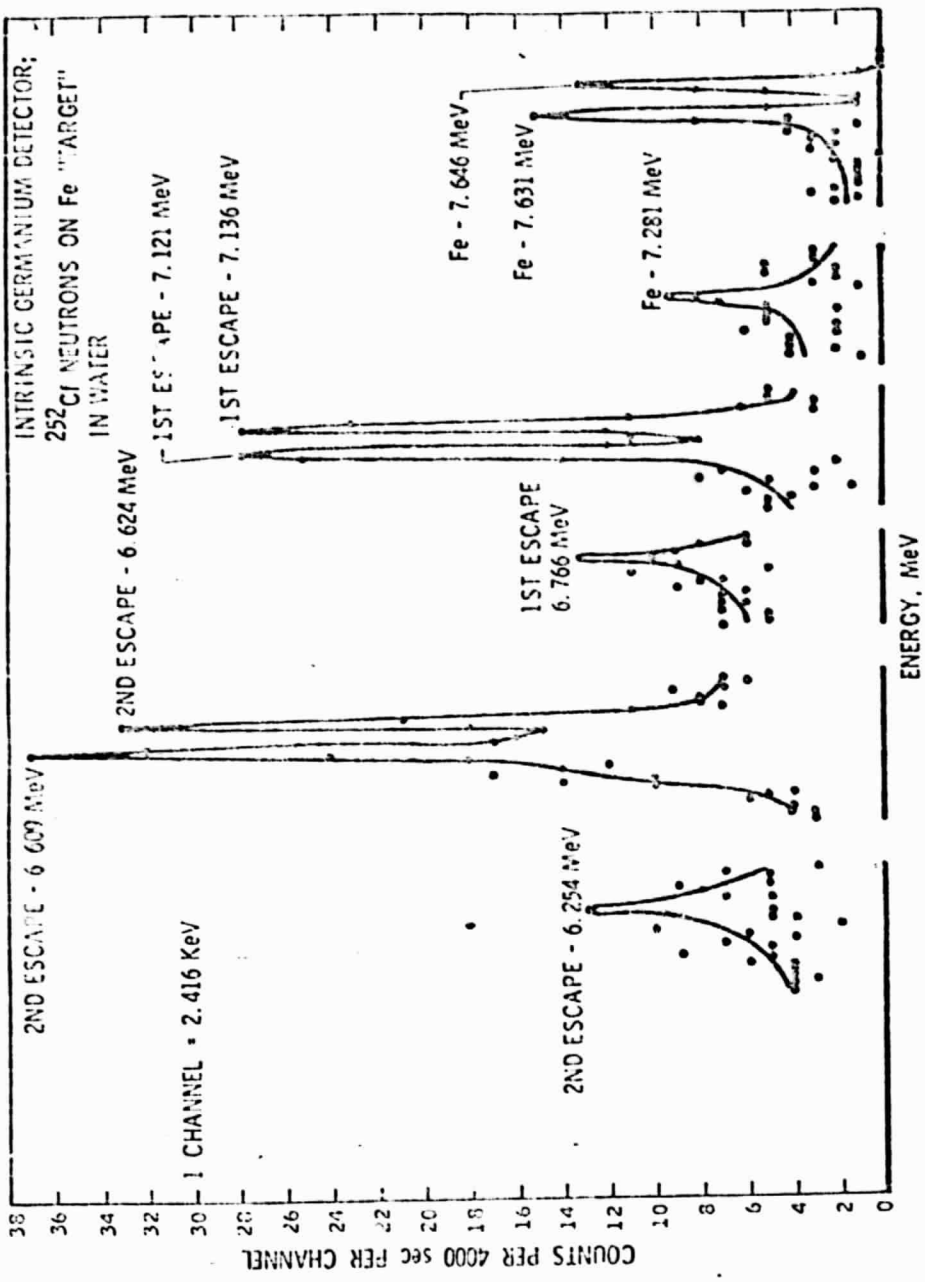
INTRINSIC GERMANIUM DETECTOR;
252Cf NEUTRONS ON Fe "TARGET"
IN WATER
2ND ESCAPE - 6.624 MeV
1ST ESCAPE - 7.121 MeV
1ST ESCAPE - 7.136 MeV
Fe - 7.646 MeV
Fe - 7.631 MeV
Fe - 7.281 MeV
1ST ESCAPE
6.766 MeV
2ND ESCAPE - 6.254 MeV
2ND ESCAPE - 6.609 MeV
1 CHANNEL = 2.416 KeV
COUNTS PER 4000 sec PER CHANNEL
ENERGY, MeV

Figure 5

ORBITING GAMMA-RAY SPECTROSCOPY

LUNAR SENSITIVITY LIMITS WITH

LARGE GERMANIUM DETECTOR

ELEMENT	OBSERVING TIME			LUNAR SOIL TYPES		
	1 hr. 3σMDL	10 hr. 3σMDL	100 hr. 3σMDL	HIGHLAND (A-16)	KREEP (A-14)	MARE (A-11)
Th PPM	0.52	0.17	0.052	2.11	14.00	2.1
U PPM	0.12	0.039	0.012	0.58	4.00	0.55
K %	0.028	0.0087	0.0028	0.096	0.430	0.115
Fe %	1.5	0.47	0.15	4.00	8.00	12.3
Ti %	0.60	0.19	0.060	0.34	1.00	4.6
Si %	3.4	1.1	0.34	21.1	22.5	20.0
O %	6.5	2.1	0.65	45.0	44.2	41.6
Al %	5.5	1.8	0.55	14.4	9.2	7.10
Mg %	3.0	0.95	0.30	3.3	5.60	4.60
Ca %	13	4.1	1.3	11.2	7.60	8.60
C %	5.4	1.7	0.54	-	-	-
N %	0.50	0.16	0.050	0.0015	0.004	0.007
Na %	1.0	0.32	0.10	0.350	0.470	0.32
Mn %	1.2	0.37	0.12	0.054	0.100	0.16
Ni %	0.79	0.25	0.079	0.045	0.040	0.024
Cr %	2.7	0.86	0.27	0.075	0.13	0.195
S %	4.9	1.5	0.49	0.060	0.10	0.10
Cl %	0.17	0.054	0.017	0.0012	0.010	0.003
Lu PPM	11	3.5	1.1	0.5	3.2	1.6
Gd PPM	250	80	25	7.00	35.00	17.00

Table 2

ORBITING GAMMA-RAY SPECTROSCOPY
MARS SENSITIVITY LIMITS WITH LARGE
GERMANIUM DETECTOR

ELEMENT	APOLLO 11 BASALT (MEAN)	SENSITIVITY (3σ) UNCOLLIMATED			COLLIMATED		
		1 hr.	10 hr.	100 hr.	1 hr.	10 hr.	100 hr.
Th PPM	2.1	1.5	0.5	0.15	2.7	0.9	0.27
U PPM	0.55	0.9	0.3	0.10	1.7	0.5	0.17
K %	0.12	0.11	0.03	0.011	0.19	0.060	0.019
Fe %	12	2.9	0.9	0.29	5.8	1.8	0.58
Ti %	5	1.2	0.4	0.12	2.4	0.8	0.24
Si %	20	11	3	1.1	22	7	2.2
O %	42	13	4	1.3	27	8	2.7
Al %	7.1	-	9	2.9	-	16	5
Mg %	4.6	-	4.0	1.2	-	7	2.2
Ca %	8.6	-	-	4.4	-	-	8
C %	(30)*	12	4	1.2	-	8	2.4
H %	(5)*	1.6	0.5	0.16	2.8	0.9	0.28
Na %	0.3	-	3	1.1	-	-	1.9
Mn %	0.2	-	0.7	0.23	-	-	0.5
Ni %	0.024	-	0.5	0.15	-	1.0	0.30
S %	0.10	-	3.0	1.0	-	-	2.0
Cl %	0.003	-	0.11	0.035	-	-	0.07
Lu PPM	2	-	-	17	-	-	29

Cr, Sr, Ba AND Gd MAY ALSO BE DETECTABLE AT THE LONGER OBSERVING TIMES

*PROJECTED POLAR CAP CONCENTRATIONS FOR MARS